

Flood Energy Dissipation in Anabranching Channels

| | |
|-------------------------------|---|
| Journal: | <i>River Research and Applications</i> |
| Manuscript ID | RRA-17-0223.R2 |
| Wiley - Manuscript type: | Research Article |
| Date Submitted by the Author: | 05-Apr-2018 |
| Complete List of Authors: | Entwistle, Neil; University of Salford, School of Environment and Life Sciences Heritage, George; AECOM, Milan, David; University of Hull, School of Environmental Sciences |
| Keywords: | Anabranching, LiDAR, Natural Flood Management, 2D hydraulic modelling |
| | |

SCHOLARONE™
Manuscripts

view

Flood Energy Dissipation in Anabranching Channels

Neil Entwistle¹, George Heritage², and David Milan*³

¹ *School of Environment and Life Sciences, University of Salford, Peel Building,
Salford, M5 4WT, UK*

² *AECOM, Exchange Court, 1 Dale Street, Liverpool, L2 2ET, UK*

³ **School of Environmental Science, University of Hull, Cottingham Road, Hull, HU6
7RX, UK, d.milan@hull.ac.uk*

1
2
3 Keywords: Anabranching; LiDAR; natural flood management

4 **Abstract**

5
6 This study examines the character of developing anabranching channel networks on
7 the River Wear, north England using metre-scale aerial LiDAR. DSM-DTM
8 interpretation reveals a well-developed vegetation structure and a locally diverse
9 terrain, dominated by an interlinked channel network split by low elevation
10 depositional areas with the gross morphology of the reach resembling that of a
11 strongly active meandering / wandering channel suggesting that an anabranching
12 network may develop within systems that were initially active meandering and
13 wandering, evolving in line with floodplain vegetative succession. Utilisation of the
14 LiDAR DEM in the hydrological component of the CAESAR-Lisflood (version 1.4)
15 morpho-dynamic model has generated local hydraulic variable estimates through the
16 anabranching reaches for a range of flows. These data clearly demonstrate how
17 elevated flows are transferred out of the primary channel and distributed along the
18 interconnected secondary channel network, creating a diverse set of hydraulic
19 environments. Areas between the channels rapidly become inundated as flows
20 increase, dissipating flow energy. Shear stress estimates throughout the study site
21 reveal a generally reduced ability to mobilise sediments and erode channel margins,
22 in comparison to a single-thread reach immediately downstream. Anabranching
23 secondary channels appear to operate in disequilibrium and act predominantly as
24 aggradational zones, although with some evidence of scour at channel bifurcation
25 and confluence points. It would appear that the topographic character of
26 anabranching sites efficiently manages flood flow energy, activating secondary
27 channels and low elevation areas to distribute flood flows. These findings contrast
28 with the hydraulic data from an adjacent single-thread reach, characterised by flood
29 flows concentrated in-channel creating a high erosive potential. We propose that
30
31
32
33
34
35
36
37
38
39
40
41
42
43
44
45
46
47
48
49
50
51
52
53
54
55
56
57
58
59
60

1
2
3 anabranching rivers could play an important role in natural flood and sediment
4 management in many UK river systems.
5
6
7

8 9 **Introduction**

10
11 Anabranching and anastomosing rivers represent a major group of rivers that exhibit
12 a multi-thread channel network divided by stable islands often colonized by woody
13 vegetation and associated with wetland areas. Despite anabranching being the
14 prevailing river pattern found along alluvial tracts of the world's largest rivers, it is the
15 least understood channel type (Jansen and Nanson, 2004). Major differences exist
16 concerning their definition (see Carling *et al.*, 2014 for a review), and the causes of
17 their existence (Kleinhans *et al.*, 2012). We follow the scheme of Nanson and
18 Knighton (1996) who treat all non-braided multi-thread channels as 'anabranching',
19 using the term to describe both low (sand-dominated) and high energy (gravel-bed)
20 multi-thread systems in their six-fold channel classification. These workers identify
21 two classes of gravel-dominated anabranching systems (Types 5 and 6); one of
22 which is laterally active. The active (Type 5) channels are analogous to wandering
23 channels (Desloges and Church, 1989), in that they often exhibit a less stable,
24 dominant channel with multiple (more stable) anabranches, and may also alternate
25 between multi- and single-thread reaches. These channels may be initiated by
26 enhanced sediment supply, and log jams, and substantial lateral activity is often a
27 feature. Nanson and Knighton (1993) also suggest that this type of anabranching
28 may be driven by the needs to maintain bedload transport efficiency. Avulsion
29 channels may form on the floodplain and fill with sediment to form large bars that
30 become colonised with vegetation (Nanson and Knighton, 1996). Type 6
31 anabranching channels are more stable and form through log jams or sediment
32
33
34
35
36
37
38
39
40
41
42
43
44
45
46
47
48
49
50
51
52
53
54
55
56
57
58
59
60

1
2
3 accumulation. The Wolsingham site is a high energy multi-thread gravel-bed river,
4 with vegetated islands displaying the character of type 5 and type 6 anabranching
5 channels to describe the study site used in this paper.
6
7
8
9

10
11 Anabranching river channels in the UK were arguably the dominant channel type
12 before historic channel management practice led to their loss, with most lowland
13 medieval rivers either inactively meandering or anabranching (Lewin, 2010). For
14 example, Lewin (2010) presents cartographic evidence for anabranching morphology
15 for tributaries of the lower Thames, specifically the Rivers Coln and Lea. Large and
16 Petts (1996) also report historic anabranching for reaches for the River Trent in
17 Nottinghamshire. Anabranching rivers are rare in the UK today and channel and
18 floodplain management practices are inhibiting their development through vegetative
19 succession suppression. However, there is evidence of a return to an anabranching
20 channel form on a number of UK rivers, and this appears to be coincident with
21 cessation of intensive floodplain management practice loci (Heritage *et al.*, 2016).
22
23
24
25
26
27
28
29
30
31
32
33
34
35
36

37 No process-based studies on anabranching systems in the UK are available in the
38 literature, possibly reflecting their rarity. On some UK rivers, localised anabranching
39 systems can occur in locations where river-floodplain interaction has been allowed to
40 occur unimpeded. They exhibit a stable multi-channel planform separated by well
41 vegetated bars and islands, however they have developed on moderate to high
42 energy gravel-dominated rivers (*sensu* Nanson and Knighton, 1996) unlike the lower
43 energy anastomosing systems transporting cohesive sediments more commonly
44 reported in the literature (Makaske, 2001). This paper investigates the energy
45 regime of an anabranching reach of the River Wear, compared with an adjacent
46
47
48
49
50
51
52
53
54
55
56
57
58
59
60

1
2
3 single-thread channel, contrasting the hydraulic forces acting to control the character
4 of each system. A 2D hydraulic model is developed to simulate these changes
5 across the flow regime.
6
7
8
9

10 11 **Methods**

12 13 **Study site characteristics**

14
15 The study focused on a 1.5 km reach of the upper river Wear at Wolsingham, County
16 Durham, UK, situated at around 140 m AOD (Figure 1a). The 171.9 km² catchment
17 upstream drains a geology of impermeable Lower Carboniferous Limestone, overlain
18 by peat in the headwaters and till and alluvium in the middle reaches. The relatively
19 low permeability of these deposits and steep upper catchment results in a flashy
20 hydrograph response. The river has been impounded in its upper reaches by
21 Burnhope reservoir, since 1937 but this does not attenuate flows. The river valley at
22 Wolsingham is dominated by two late glacial and three Holocene terraces (Moore,
23 1994). The river bed at Wolsingham has a mean channel gradient of 0.007 m/m.
24
25
26
27
28
29
30
31
32
33
34
35
36
37

38 Figure 1
39
40
41

42 43 **Remote Sensing Information**

44
45 Interrogation of the 1 m resolution LiDAR DTM for the study reach, sourced from the
46 UK EA Geomatics group, reveals a well-developed channel network, not at first
47 visible from the DSM and aerial imagery (available for 1951, 1957, 1971, 2007,
48 Wishart et al., 2008; Googleearth, 2016) of the reach due to dense riparian vegetation
49 cover (Figure 1b,c).
50
51
52
53
54
55
56
57
58
59
60

Hydrological data

Figure 2a shows the $62 \text{ m}^3\text{s}^{-1}$ peak over threshold series for the river Wear recorded at Stanhope, sourced from the UK Environment Agency, situated 8 km upstream of the study site. These data are translated into an annual maximum return period curve (Figure 2b). The mean daily discharge recorded at Stanhope situated upstream of the study site is $3.92 \text{ m}^3\text{s}^{-1}$ (Wishart et al., 2008). Daily flow statistics show that flows of $0.5 \text{ m}^3\text{s}^{-1}$ are exceeded 95% of the time, and flows of $9.3 \text{ m}^3\text{s}^{-1}$ are exceeded 10% of the time (Figure 2b). The 2-yr return period discharge, approximately equivalent to the bankfull flow (Hey, 1975) for the channel in regime, is $124.5 \text{ m}^3\text{s}^{-1}$. Data for peak flows (Figure 2a) indicate the most significant event in the historic flood series to be in 2005 (approaching $247 \text{ m}^3\text{s}^{-1}$). However Wishart et al. (2008) indicate that a higher event of $297 \text{ m}^3\text{s}^{-1}$ occurred in 1958.

Figure 2

Fluvial Audit

A fluvial audit (*sensu* Sear et al., 1995) was conducted along the study reach gathering observation-based evidence of current and former channel form and the influence of controlling processes. This revealed strong connectivity between the primary channel and adjacent riparian zone through the anabranch section, this connectivity reduced significantly through the single-thread reach downstream with the channel here displaying an inset character and a disconnected floodplain. The loose nature of the bed material suggests strong active transport along the river and

1
2
3 flood flows had delivered some of this sediment through to secondary channels in
4 the anabranching reach where they were forming functioning riffle and bar units. Fine
5 sediment is also being transported through both channel types and was seen to
6 accumulate in the bed and as marginal deposits, some of which were becoming
7 consolidated. Many of the anabranching reach secondary channels only flow during
8 elevated discharge and are otherwise characterised by residual isolated pools
9 throughout most of the year. Large woody debris was common along the secondary
10 channels forming stable features around which flow bifurcated. These features
11 appear to exert some control on secondary channel development in the
12 anabranching area. Woody debris was absent in the single-thread reach. Vegetation
13 in the anabranching zone is characterised by mature ash, and sycamore woodland
14 (Figure 3c) with smaller numbers of younger alder and willow closer to the main
15 channel. An understory of shrub, bramble and ruderals are present across most of
16 the site. This contrasts with a thin and disrupted woody riparian strip along the single
17 thread section. Bank erosion was noted along both channel types, but was more
18 prevalent through the single-thread reach.
19
20
21
22
23
24
25
26
27
28
29
30
31
32
33
34
35
36
37
38
39

40 Figure 3

41 42 43 44 Historical channel changes

45
46 Commercial gravel extraction took place at a number of locations on the Wear,
47 including the site at Wolsingham, during the 20th century involving intensive channel
48 and floodplain management with periodic re-routing of flow allowing new areas of
49 bed to be worked, and encouraging former pits to be refilled with sediment (Wishart
50 *et al.*, 2008). Cessation of gravel mining from the river at the site in the 1950s has
51
52
53
54
55
56
57
58
59
60

1
2
3 allowed natural processes to operate with recovery towards a stable wooded
4 anabranching system consisting of a dominant channel and multiple secondary
5 channels. This unmanaged naturalisation of the watercourse developing a well-
6 connected floodplain area across the former widened mined reach is a key factor
7 behind the historical channel recovery shown in Figure 4. The multiple secondary
8 channels are not evident when viewing the 2007 aerial photograph due to dense
9 woodland development, however they are visible on the LiDAR DTM (Figure 1b).
10
11 Away from the mined reach progressive channel incision has disconnected the
12 single thread channel from its floodplain.
13
14
15
16
17
18
19
20
21
22
23

24 Figure 4

25
26
27
28
29 There is a good historic record of morphodynamism for study reach that dates back
30 to the early Tithe maps of 1839. Wishart *et al.* (2008) documents channel change for
31 Wolsingham and a second site on the Wear at Harperley Park, using historic maps
32 and aerial photographs for the period 1839-1991, and makes tentative links between
33 channel changes and piecemeal gravel extraction. Aerial photographs for the site
34 dating from 1951 are shown in Figure 4. The 1951 image clearly demonstrates the
35 channel to be a dynamic multi-thread system, displaying a wandering channel
36 morphology, with a combination of active mid-channel bars and some more stable
37 vegetated islands. The 1957 image appears to show a less active channel; with
38 some of the active bars become vegetated and more stable. The channel appears
39 largely single-thread in nature, however the vegetation masks a stable multi-thread
40 system beneath, that is only inundated during high flow events. The 1971 image
41 (Figure 4) shows a more confined channel with some mid-channel bars. Some of the
42
43
44
45
46
47
48
49
50
51
52
53
54
55
56
57
58
59
60

1
2
3 old abandoned channels are being farmed, and others have become well-vegetated.
4
5 The channel is anabranching towards the downstream end of the reach, with well-
6
7 vegetated islands. By 2007 there is a dominant channel, with occasional transverse
8
9 bars, and the anabranching section is covered in dense vegetation. All of the old
10
11 multi-channel network is now part of the wooded anabranching reach, activated at
12
13 higher flows, further revealed on the LiDAR DTM (Figure 1b).
14
15
16
17
18
19

20 Hydraulic modelling

21
22 CAESAR-Lisflood (version 1.4) was used in reach mode to simulate depth-averaged
23
24 hydraulics (Coulthard *et al.* 2013). The hydrodynamic flow model is based on the
25
26 Lisflood FP code (Bates and De Roo, 2000), that conserves mass and partial
27
28 momentum, and simulates in-channel hydraulic processes. Although Lisflood FP is
29
30 primarily used as a flood inundation model it has also been used to examine channel
31
32 morphodynamics (Wong *et al.*, 2015). The LISFLOOD-FP component of CAESAR-
33
34 Lisflood is a one-dimensional inertial model derived from the full shallow water
35
36 equations that is applied in the x and y directions to simulate two dimensional flow
37
38 over a raster grid (Coulthard *et al.*, 2013). As such CAESAR-Lisflood simulations
39
40 must be regarded as only a first approximation to the problem, however Bates *et al.*
41
42 (2010) and Neal *et al.* (2011) demonstrated that the model was capable of simulating
43
44 flow depths and velocities within 10% of a range of industry full shallow water codes.
45
46 Their simulations of gradually varying flows, revealed that velocity predictions were
47
48 'surprisingly similar' between the models and they suggest that Lisflood-FP model
49
50 may be appropriate for velocity simulation across a range of gradually varied
51
52 subcritical flow conditions.
53
54
55
56
57
58
59
60

1
2
3
4
5 Bare-earth LiDAR, sourced from the EA Geomatics group was used to produce a 1-
6 m DEM for the study reach (Figure 1b). Surface grain size for the study reach
7 measured using grid-by number sampling (Wolman, 1954), revealed a reach D_{50} of
8 65 mm, D_{84} of 107 mm, and D_{99} of 175 mm; generally coarser than the bulk sample
9 grain size reported by Wishart *et al.* (2008). A general Mannings 'n' grain scale
10 roughness value of 0.03 was calculated using the Strickler equation ($n=D^{1/6}/21$),
11 where D is the D_{50} surface grain size, and this was used in the simulations.
12 Additional form roughness variation in the form of morphology and planform variation
13 is implicitly represented by topographic variation in the DEM. Given the small grid
14 cell size a Courant Number of 0.3 was chosen to avoid computational model stability
15 issues. The calculated Froude Number was limited to the default value of 0.8 and
16 horizontal water flux threshold was also left as the default value of 0.00001 m. The
17 flow model was then run for a range of hydrographs ranging from $16 \text{ m}^3\text{s}^{-1}$,
18 equivalent to the daily flow exceeded 5% of the time (Figure 2b) and $198 \text{ m}^3\text{s}^{-1}$,
19 approximately equivalent to the 40 yr return period. This flow remained in-bank along
20 the inset single-thread sections of channel, however fully inundates the anabranching
21 section.

22
23
24
25
26
27
28
29
30
31
32
33
34
35
36
37
38
39
40
41
42
43
44 The model was validated against dGPS, water surface height measurements taken
45 at two different low flow gauged discharges ($5.2 \text{ m}^3\text{s}^{-1}$ and $7.8 \text{ m}^3\text{s}^{-1}$ at three locations
46 along the study reach. These elevation measurements were compared with
47 simulated water surface elevations at the measurement points at equivalent
48 discharges. Elevation differences were found to be ± 0.01 m of the measured values
49 (Table 1). For these flows, the data suggest that the modelling provides a good
50
51
52
53
54
55
56
57
58
59
60

1
2
3 estimate of channel hydraulics, based upon the water surface representing the
4 hydraulic integrity of the reach. No high flow hydraulic measurements were taken at
5 the site, however, a peak flood strandline estimate for the river (5/12/2012) was
6 obtained from internet imagery (Glenister, 2015), at Causeway Road Bridge located
7 in between the anabranching and single thread reaches (Figure 5). This strand
8 equated to a peak flow discharge of $159.45 \text{ m}^3\text{s}^{-1}$ measured at Stanhope Weir gauge
9 station.
10
11
12
13
14
15
16
17
18
19

20 Table 1

21 Figure 5
22
23
24
25

26 The strand line is composed of fragments of woody vegetation that have collected in
27 the low energy lee zone after the bridge abutment and was locally well defined
28 following the contour line of the tarmac path next to the river. The elevation of the
29 debris was found to be 136.4 masl from EA LiDAR of the reach (Figure 5). A stage –
30 discharge relationship was developed for the open water area close to the bridge
31 from the multiple water surface simulations output from CAESAR Lisflood (Figure 5)
32 and a discharge of $163.44 \text{ m}^3\text{s}^{-1}$ obtained for the strandline elevation. This is a 2.5%
33 overestimation compared to the gauge.
34
35
36
37
38
39
40
41
42
43
44
45

46 Depth average velocity output from each simulation was then used to estimate point
47 shear stress (τ_o) using Wilcock's (1996) equation
48
49
50
51

$$\frac{U}{u_*} = \frac{1}{\kappa} \ln \left(\frac{h}{\ell z_0} \right)$$

(1)

where the shear velocity $u_* = (\tau_o / \rho)^{1/2}$, ρ is water density, U is depth average velocity, κ is von Karmens constant (taken to be 0.4), ℓ is the base of the natural logarithms, h is local water depth, z_0 is an estimate of bed roughness. Under appropriate flow conditions an estimate of u_* termed u_{*h} may be derived using (1), using simulated values of U and h . When both grain and form roughness exist, u_{*h} is the total drag composed of both form drag and skin friction (Wilcock, 1996). Using this approach, Wilcock (1996) found that local bed shear stress was estimated to within 3% of that measured where relatively simple flow geometries were involved.

Predictions of depth and shear stress were computed at a 1 m² resolution across the channel and then were visualised in SURFER (Figure 6) Comparisons were made between the anabranching upstream reach and the downstream single-thread reach. Unit shear stress (shear stress per unit area) and total shear stress (summation of shear stress values for channel segments) were calculated using the 1 m² 2D hydraulic model outputs for each of these sub-reaches for the full range of simulations, in order that comparisons in energy between the two channel styles could be made.

Figure 6

Results

Flow depth and shear stress patterns

1
2
3 Figure 6a shows flow depth and areal inundation extent throughout the study reach
4 over the flow regime, demonstrating how the abandoned multi-thread channel areas
5 of the anabranching reach gradually become inundated with increasing flood peaks.
6
7 Progressive inundation characteristics for the anabranching and single-thread sub-
8 reaches are shown for the range of simulated flows in Figure 6, and clearly illustrate
9 the contrasting response to flood flows between the two channel types. The
10 anabranching reach doubles its flow area at $68 \text{ m}^3\text{s}^{-1}$, as one of the secondary
11 channels becomes inundated, whilst the flow area within the single-thread reach
12 remains approximately constant (Figure 6a). Downstream of the anabranching
13 reach, confinement of flow to single-thread morphology results in significantly greater
14 flow depths compared with the anabranching reach, for a comparative discharge
15 (Figure 6a). Flow concentration and resultant greater flow depths in the single-
16 thread reach increase the probability of sediment transport, and erosion of the bed
17 and banks. These findings suggest that the single-thread reach is strongly inset
18 within the floodplain, and is no longer functionally connected to its floodplain.
19 However the anabranching section behaves differently; with a primary channel at low
20 flow and an ephemeral multithread secondary channel network and wooded zone,
21 that acts as a new floodplain level during high flows.
22
23
24
25
26
27
28
29
30
31
32
33
34
35
36
37
38
39
40
41
42
43

44 The spatial distribution of shear stress throughout the study reach shown in Figure
45 6b, demonstrates how energy appears to be dissipated through the anabranching
46 channels as flood stage rises. The highest shear stress peaks have a tendency to be
47 located in the single-thread reach. In the anabranching section, shear stresses tend
48 to be low at channel heads and higher at downstream channel confluences. This
49 can be seen on a local scale for the $198 \text{ m}^3 \text{ s}^{-1}$ simulation (Figure 6c). Differences in
50
51
52
53
54
55
56
57
58
59
60

1
2
3 shear stress between anabranching and single-thread sections are revealed
4 graphically through a plot of simulated shear stress for the high flow ($198 \text{ m}^3\text{s}^{-1}$)
5 plotted against distance downstream along the channel thalweg in Figure 7. Typical
6 shear stress values are below 80 Nm^{-2} in the anabranching section, compared with a
7 much more variable pattern shown for the single-thread section; with peaks in
8 excess of 200 Nm^{-2} . Kurtosis and skewness statistics based upon the distribution of
9 shear stress values over the range of simulated flows further highlight differences
10 between the single-thread and anabranching reaches (Figure 8). Although both
11 reaches show a decline in both Kurtosis and skewness as flow increases, the single-
12 thread reach consistently demonstrates greater kurtosis and skewness, suggesting
13 that shear stress values are concentrated into a narrower range, and are skewed
14 towards higher shear stress values compared with the anabranching reach. This
15 suggests that the single-thread reach should have greater sediment transport
16 potential and potential to scour its bed and banks. The flattening out of the curves
17 for the anabranching reach in Figure 8a and b, suggests a wider range (less skewed)
18 of shear stresses are exerted on the bed and banks, and less peaked distribution, at
19 flows in excess of around $60 \text{ m}^3\text{s}^{-1}$. This could reflect the effects of bar
20 submergence.

21
22
23
24
25
26
27
28
29
30
31
32
33
34
35
36
37
38
39
40
41
42
43
44 Figure 7

45
46 Figure 8

47 48 49 50 Sediment transport potential

51
52
53 The geomorphic effectiveness of the shear stress patterns may be assessed through
54 comparing the simulated shear stress relative to the critical shear stresses (τ_c) for
55
56
57
58
59
60

1
2
3 bedload movement, calculated from the reach-scale surface grain-size
4 characteristics
5

$$\tau_c = \theta(\rho_s - \rho)gD_{50} \quad (2)$$

6
7
8
9
10
11
12
13 where θ is the critical dimensionless shear stress (0.047), ρ_s is the sediment density,
14 ρ is the fluid density, g is acceleration due to gravity, and D_{50} is the median surface
15 grain-size. Typically shear stresses did not exceed 100 N m^{-2} in the anabranching
16 sub-reach, and suggest partial mobilisation of material up to the D_{50} , however was
17 insufficient to mobilise grain sizes of the D_{50} and above (Figure 7). Low shear
18 stresses are indicative of a generally stable bed during flood conditions for the
19 anabranching sub-reach, and a trend towards aggradation. However, where the flow
20 is confined into a single-thread channel downstream, shear stresses are significantly
21 greater, peaking at close on 250 Nm^{-2} . This shear stress is sufficient to mobilise bed
22 material around the D_{84} percentile in a number of locations along this reach,
23 suggesting a near fully mobile bed and a much greater potential for morphological
24 change. This also helps to explain the incised nature of the single-thread reach,
25 apparent from the LiDAR DEM. Evidence of bank erosion is also evident at a
26 number of locations along the single-thread section, possibly in response to incision.
27
28
29
30
31
32
33
34
35
36
37
38
39
40
41
42
43
44
45

46 Total shear stress for both single-thread and anabranching channel styles are plotted
47 against discharge in Fig 9a, revealing that the anabranching reach is indicative of
48 consistently greater energy over the flow regime compared with the single-thread
49 reach downstream. However the anabranching reach has a much greater flow area
50 in comparison to the single-thread reach. When shear stress is scaled by unit area, a
51
52
53
54
55
56
57
58
59
60

1
2
3 very different picture is evident, with flow energy consistently lower in the
4
5 anabranching reach (Figure 9b). Lower unit shear stress data demonstrates that
6
7 energy is dissipated more effectively in the anabranching reach. At higher
8
9 discharges flow is diverted into the anabranching channel network, flowing over a
10
11 greater surface area compared with a single-thread channel, with increased overall
12
13 roughness, including the influence of vegetation roughness; further resulting in
14
15 energy loss. The initial rate of increase in unit shear stress up until $36 \text{ m}^3\text{s}^{-1}$ is
16
17 greater for both anabranching and single-thread sections, possibly reflecting flow
18
19 contained within the dominant channel throughout the study reach. At flows beyond
20
21 $36 \text{ m}^3\text{s}^{-1}$, the anabranching section starts to becoming inundated, and this influences
22
23 the rate of unit shear stress increase both within the anabranching and single thread
24
25 section downstream. In general the rate of unit shear stress increase with discharge
26
27 is greater for the single-thread section, reflecting the effects of the smaller channel
28
29 cross-section area.
30
31
32
33
34

35 Figure 9
36
37
38
39

40 Potential for morphological change 41

42 Potential scour maps, indicating the areas that exceed the critical shear stress to
43
44 mobilise the D_{50} , are shown for each flow simulation in Figure 10. Potential for scour
45
46 of the surface bed sediments is almost exclusively confined to the single-thread
47
48 section of channels, and parts of the primary channel that runs through the
49
50 anabranching section. As discharge rises, the shear stress capable of mobilising the
51
52 bed surface gradually increases. Areas of potential bed mobilization are very patchy
53
54 for the lower discharge simulations, however progressively greater areas of the bed
55
56
57
58
59
60

1
2
3 are susceptible for mobilization with increasing flow. The majority of the secondary
4 channels in the anabranching section consistently appear unable to transport bed
5 surface sediments, however for flows in excess of $96 \text{ m}^3\text{s}^{-1}$, the tail end of the
6 secondary channel system, just before it rejoins the primary channel, does appear to
7 show potential for bed scour. The spatial patterns shown, suggest that bed material
8 fed in to the secondary channels from upstream, is likely to stall in the channel
9 network, whilst the downstream end may see some headward progressing incision.
10 In effect the secondary channels are in disequilibrium with the rest of the system,
11 and both these mechanisms provide potential pathways for avulsion. The primary
12 channel running through the anabranching section, generally appears efficient at
13 mobilizing bed surface sediments.
14
15
16
17
18
19
20
21
22
23
24
25
26
27
28

29 Figure 10
30
31
32
33
34

35 Discussion

36
37 Research focused on the hydraulic characteristics of anabranching channels are
38 limited (e.g. Harwood and Brown, 1993; Jansen and Nanson, 2004; Makaske *et al.*,
39 2009), with the majority of studies focussing upon the morphodynamics of these
40 systems (e.g. Knighton and Nanson, 1996; Makaske, 2001; Burge, 2006; Huang and
41 Nanson, 2007; Kleinhans *et al.*, 2012). This paper has compared the hydraulic
42 characteristics of anabranching and single-thread morphology. A clear contrast in
43 hydraulic behaviour was simulated across the flow regime, with the single-thread
44 reach displaying consistently higher shear stresses. The anabranching reach had a
45 primary channel with lower shear stresses compared to the single-thread reach
46
47
48
49
50
51
52
53
54
55
56
57
58
59
60

1
2
3 downstream, and a secondary system of anabranches that start being inundated at
4 flows in excess of $36 \text{ m}^3\text{s}^{-1}$ (Return Period 0.4 years). These were characterised
5 initially by very low shear stresses, before exhibiting higher values at anabranch
6 confluences in the higher flow simulations, analogous to Harwood and Brown's
7 (1993) findings on the Gearagh, wooded anabranch system on the River Lee,
8 Ireland.
9
10
11
12
13
14
15
16
17

18 Our findings also indicate strongly contrasting channel-floodplain connectivity
19 between the two adjacent reaches. Interrogation of historical photographs and maps
20 suggests that the single-thread section was previously active, with mobile gravel
21 bars. Gravel mining is likely to have resulted in sediment starvation to the single-
22 thread reach downstream, and promoted incision. Since the 1970s these have been
23 vegetated and stabilised, with much less evidence of lateral instability, further
24 reducing sediment supply. It is likely that the single-thread reach has incised as a
25 result of shear stresses capable of mobilising the surface bed material, and the
26 channel has become disconnected from its former floodplain: flow remained within
27 the channel even at the highest simulation ($198 \text{ m}^3\text{s}^{-1}$). The anabranching reach
28 begins to inundate floodplain sub-channels at around $35 \text{ m}^3\text{s}^{-1}$; a value well below
29 the traditional bankfull return period occurring on 5 days/yr on average (Hey, 1975).
30 Anabranching channels typically flood overbank more frequently than single-thread
31 channels, resulting in greater sediment delivery to floodplains and island-ridges
32 flanking the anabranches (Jansen and Nanson, 2004).
33
34
35
36
37
38
39
40
41
42
43
44
45
46
47
48
49
50
51

52 Unit shear stress results for the study site also suggest a marked contrast, with the
53 anabranching reach rapidly dissipating energy across the multithread sub-channel
54
55
56
57
58
59
60

1
2
3 network during elevated flows. Jansen and Nanson (2004) report similar
4 observations for Magela Creek, and suggest that anabranching morphology is more
5 efficient at using excess energy at high stage, through dissipating the energy over
6 the multiple channel network, where it is met with higher roughness in comparison
7 with single-thread channels. Interestingly Jansen and Nanson (2004) suggest
8 stream power between the two channel sub-reaches diverge at discharges above
9 bankfull. At the Wolsingham site, shear stresses diverge at discharges well below
10 bankfull. Essentially the shear stresses are always greater in the single-thread
11 section, as flow depth is greater and channel width narrower, in comparison to the
12 anabranch section. For a given increase in discharge, the rate of increase in
13 shear stress is consistently greater in the single-thread section, as channel width
14 does not change as significantly as it does in the anabranch section, and flow
15 depths increase at a faster rate in the single-thread section due to flow confinement.
16
17
18
19
20
21
22
23
24
25
26
27
28
29
30
31
32

33 Shear stresses in the anabranch section do not appear competent enough to
34 mobilise the surface D_{50} at peak flows throughout the network of secondary
35 channels. However evidence from the fluvial audit (Figure 3a) indicates that some
36 bedload is fed into, and deposited in some of the secondary channels suggesting a
37 degree of transport and potential slow aggradation. Huang and Nanson (2007) have
38 shown that increasing the number of channels without adjusting channel slope can
39 lead to a proportional decrease in flow efficiency, and hence sediment transport
40 capacity. It is likely that the secondary channels in the anabranching section at
41 Wolsingham are aggradational, and hence in disequilibrium (*sensu* Makaske *et al.*,
42 2009). Aggradational disequilibrium anabranch systems may transport and stored
43
44
45
46
47
48
49
50
51
52
53
54
55
56
57
58
59
60

1
2
3 sediment through a continual process of channel creation and old channel
4 abandonment (Huang and Nanson, 2007)
5
6
7

8
9 It would appear that the anabranching reach at Wolsingham has developed following
10 the cessation of intensive channel management (gravel extraction, grazing and wood
11 management), allowing barforms to stabilise through vegetative succession. A
12 diverse mosaic of vegetation can potentially develop, an observation shown for
13 wandering channel morphology on the river Feshie by Gilvear and Willby (2006).
14 The diversity in hydraulic conditions modelled for the Wolsingham site have the
15 potential to support an unusually varied biota and range of environmental processes
16 (Naiman and Dechamps, 1997).
17
18
19
20
21
22
23
24
25
26
27

28 The overall evidence from our 2D hydraulic modelling suggests a hydraulic regime
29 broadly commensurate with sediment transport processes, however more extreme
30 flows display a hydraulic diversity which promotes morphological change, enhanced
31 by the local hydraulic effects of the vegetation, for example dead wood (Gurnell,
32 2014). It is clear that bedload can be fed in to the anabranches at high flow, which
33 could induce avulsion, through channel blockage, erosion and activation of new
34 channels through existing islands or floodplain.
35
36
37
38
39
40
41
42
43
44
45

46 Locally anabranching sections on rivers appear to be important for regulating energy
47 along the river long-profile. Although our work suggests local disequilibrium within
48 the anabranching section itself, when the full reach is considered, including the
49 single-thread section, the anabranching section could be important for maintaining
50 channel stability. Referring to the Columbia River, Huang and Nanson (2007)
51
52
53
54
55
56
57
58
59
60

1
2
3 suggest that anabranching may be the most efficient means of accomplishing
4 sediment sequestration across an aggrading floodplain. Without anabranching,
5 bedload forced through a single-thread channel may lead to a much less stable
6 condition. In a single-thread channel a significant reduction in channel width results
7 in flow confinement and increased shear, that could induce bank instability. Hence
8 retention and management of locally anabranching sites on UK rivers, could be
9 important for maintain quasi-equilibrium, when considering longer reaches. In
10 addition, their increased storage capacity, when compared with single-thread
11 sections, means that locally anabranching sections of river channel have the
12 potential to provide an important natural flood management tool.
13
14
15
16
17
18
19
20
21
22
23
24
25

26 **Conclusions**

27
28
29 The topographic character of anabranching channels efficiently manages flood flow
30 energy, activating secondary channels and low elevation areas to distribute flood
31 flows; creating a dynamically stable river environment. These findings contrast with
32 the hydraulic data from an adjacent single-thread sub-reach, characterised by
33 concentrated flood flows and a high erosive potential. In particular, anabranching
34 channels
35
36
37
38
39
40
41
42
43

- 44 • flood overbank more frequently than single-thread channels
- 45 • are less energetic than single-thread channels and the channel form,
46 are aggradational and in disequilibrium
- 47 • have a significantly more diverse hydraulic diversity in comparison to
48
49
50
51
52
53
54
55
56
57
58
59
60

- 1
2
3 • are the most common channel type on the worlds largest rivers, and
4
5 there appears to be evidence that anabranching reaches are developing at a
6
7 number of UK sites where intensive floodplain management has been
8
9 abandoned.
10

11
12
13 The site at Wolsingham suggests that anabranching reaches will develop naturally
14
15 where lateral connectivity is strong and floodplain utilisation is low allowing
16
17 vegetation succession to progress. This channel type has potential therefore for
18
19 increasing biodiversity of UK watercourses, inducing the provision of rare or
20
21 endangered habitat. An associated riparian fauna, including wading birds, fish and
22
23 amphibians will also thrive in this habitat. Therefore, allowing vegetation
24
25 development would not only have a beneficial effect for flood management purposes,
26
27 but would also enhance riparian habitat.
28
29
30
31
32
33
34

35 **References**

36
37
38 Bates P, De Roo P. 2000. A simple raster-based model for flood inundation
39
40 simulation. *Journal of Hydrology* **236**: 54–77.

41
42 Bates, P, Horritt, Ms, & Fretwell, J. 2010. A simple inertial formulation of the shallow
43
44 water equations for efficient two-dimensional flood inundation modelling, *Journal of*
45
46 *Hydrology*, **387 (1-2)**, 33-45

47
48 Burge, L. 2006. Stability, morphology and surface grain size patterns of channel
49
50 bifurcation in gravel-cobble bedded anabranching rivers. *Earth Surface Processes*
51
52 *and Landforms*, **31**, 1211-1226.
53
54
55
56
57
58
59
60

1
2
3 Carling P, Jansen J, Meshkova L. 2014. Multichannel rivers: their definition and
4 classification. *Earth Surface Processes and Landforms* **39**: 26-37.

5
6
7 Coulthard TJ, Neal JC, Bates PD, Ramirez J, Almeida GAM, Hancock GR. 2013.
8
9 Integrating the LISFLOOD-FP 2D hydrodynamic model with the CAESAR model:
10
11 implications for modelling landscape evolution. *Earth Surface Processes and*
12
13 *Landforms* **38**: 1897-1906

14
15
16 Gilvear D, Willby N. 2006. Channel dynamics and geomorphic variability as controls
17
18 on gravel bar vegetation; River Tummel, Scotland. *River Research and Applications*
19
20 **22**: 457-474.

21
22
23 Gregory SV, Boyer KL, Gurnell A (Eds.). 2003. *The ecology and management of*
24
25 *wood in world rivers*. American Fisheries Society, Symposium 37, Bethesda,
26
27 Maryland.

28
29
30 Gurnell A. 2014. Plants as river system engineers. *Earth Surface Processes and*
31
32 *Landforms* **39**: 4-25.

33
34
35 Harwood K, Brown AG. 1993. Fluvial processes in a forested anabranching
36
37 river: flood partitioning and changing flow patterns. *Earth Surface Processes and*
38
39 *Landforms* **18**: 741-748.

40
41
42 Heritage GL, Entwistle N, Milan D. 2016. Alluvial Anastomosed Channels: The
43
44 preferred channel type on active UK rivers. Proceedings of the 11th ISE Symposium,
45
46 Melbourne, Australia.

47
48
49 Hey RD. 1975. Design discharge for natural channels. In: RD Hey, TD Davies
50
51 (eds.) *Science, Technology and Environmental Management*, Saxon House, 73-88.

52
53
54 Jansen JD, Nanson GC. 2004. Anabranching and maximum flow efficiency in
55
56 Magela Creek, northern Australia. *Water Resources Research* **40**: W04503,
57
58 doi:10.1029/2003WR002408.

1
2
3 Huang, HQ, Nanson, GC. 2007. Why some rivers develop an anabranching pattern.
4
5 *Water Resources Research*, **43**, WO7441.

6
7 Kleinhans MG, de Haas T, Lavooi E, Makaske, B. 2012. Evaluating competing
8
9 hypotheses for the origin and dynamics of river anastomosis. *Earth Surface*
10
11 *Processes and Landforms* **37**: 1337-1351.

12
13 Knighton AD, Nanson GC. 1993. Anastomosis and the continuum of channel
14
15 pattern. *Earth Surface Processes and Landforms* **18**: 613-625.

16
17 Large ARG, Petts GE. 1996. Historical channel-floodplain dynamics along the River
18
19 Trent: implications for rehabilitation. *Applied Geography* **16**: 191-209.

20
21 Lewin J. 2010. Medieval environmental impacts and feedbacks: the lowland
22
23 floodplains of England and Wales. *Geoarchaeology: An International Journal* **25**:
24
25 267-311.

26
27 Makaske B. 2001. Anabranching rivers: a review of their classification, origin and
28
29 sedimentary products. *Earth Science Reviews* **53**: 149-196.

30
31 Moore EN. 1994. Glacial Geology and Geomorphology of Weardale. Unpublished
32
33 PhD Thesis, University of Durham, UK.

34
35 Naiman RJ, Décamps H. 1997. The ecology of interfaces—riparian zones. *Annual*
36
37 *Review of Ecology and Systematics* **28**: 621-658.

38
39 Nanson GC, Knighton AD. 1996. Anabranching rivers: their cause, character and
40
41 classification. *Earth Surface Processes and Landforms* **21**: 217-239.

42
43 Neal, J., Villanueva, I., Wright, N., Willis, T., Fewtrell, T. and Bates, P. (2012), How
44
45 much physical complexity is needed to model flood inundation?. *Hydrol. Process.*,
46
47 26: 2264–2282.

48
49 Sear DA, Newson MD, Brooks A. 1995. Sediment related river maintenance: the role
50
51 of fluvial geomorphology. *Earth Surface Processes and Landforms* **20**, 629-647.

1
2
3 Wilcock, P.R. 1996. Estimating local bed shear stress from velocity observations,
4
5 *Water Resources Research*, **32**(11), 3361-3366.

6
7 Glenister D. 2015. Storm Desmond – River Wear Wolsingham 2015. Available at:
8
9 <https://www.youtube.com/watch?v=bZgH5PvaO-g> [Accessed 27 March 2018].

10
11 Wishart D, Warburton J, Bracken L. 2008. Gravel extraction and planform change
12
13 in a wandering gravel-bed river: the Wear, Northern England. *Geomorphology* **94**:
14
15 131-152.

16
17
18 Wong JS, Freer JE, Bates PD, Sear DA, Step E. 2015. Sensitivity of a hydraulic
19
20 model to channel erosion uncertainty during extreme flooding. *Hydrological*
21
22 *Processes* **29**: 261-279.

23
24 Wolman MG. 1954. A method of sampling coarse river gravels. *Trans., Am.*
25
26 *Geophys. Union* **35**: 951–956.

List of Figures

Figure 1 River Wear catchment, and study reach at Wolsingham a) Catchment map, b) LiDAR image of study reach. The location of the high flow validation measurement (reported in Figure 5) is indicated by the red star and is positioned immediately downstream of the Causeway Road Bridge in Wolsingham.

Figure 2 Flow data for the River Wear at Stanhope, a) Annual Flood peak series, b) Flow frequency curve.

Figure 3 Anabranching study reach; a) Low flow channel with fresh gravel, indicative of high energy transport at higher flows, b) variety of vegetation, c) inundation of ephemeral anabranches during a flood event, d) low energy distributary with fine sediment deposition.

Figure 4 Aerial photographs for the study reach highlighting a transition from wandering, through to stabilizing anabranching to fully anabranching river type, highlighted in red on the 2007 image (Googleearth.co.uk).

Figure 5 a) Location of high flow validation immediately downstream of the Causeway Road Bridge in Wolsingham, with high flow strand-line debris visible in the bottom right corner of the image (Glenister, 2015). b) Stage-discharge curve is plotted for this site using results from our simulations. Water level data for the 5th December 2015 returned a discharge of $159.45 \text{ m}^3\text{s}^{-1}$; within 2.5% of the actual recorded at Stanhope Weir gauging station.

1
2
3 Figure 6 Results CAESAR-Lisflood model runs, demonstrating a) flow depth and
4 inundation of the anabranching channel network with increasing discharge, b) Spatial
5 patterns of shear stress through the reach, c) close-up of shear stress patterns for
6
7
8
9 198 m³s⁻¹ simulation.
10

11
12
13
14
15 Figure 7 Downstream variations in average shear stress for the 198 m³s⁻¹ simulation,
16 demonstrating significantly lower shear stress peaks, and less variability in shear
17 stress in the anabranching reach, compared with single-thread downstream. Grey
18 line is the running mean.
19
20
21
22
23

24
25
26 Figure 8 Summary statistics for shear stress over the flow regime for the single-
27 thread and anabranching subreaches, a) Kurtosis, b) Skewness.
28
29
30

31
32 Figure 9 a) Total shear stress for adjacent anabranching and single-thread reaches,
33
34 b) Unit shear stress over the flow regime for study reaches.
35
36
37

38
39 Figure 10 Spatial patterns of scour potential through the study reach based upon the
40 critical shear stress for entrainment of the bed surface D_{50} .
41
42
43
44
45
46
47
48
49
50

51 **List of Tables**

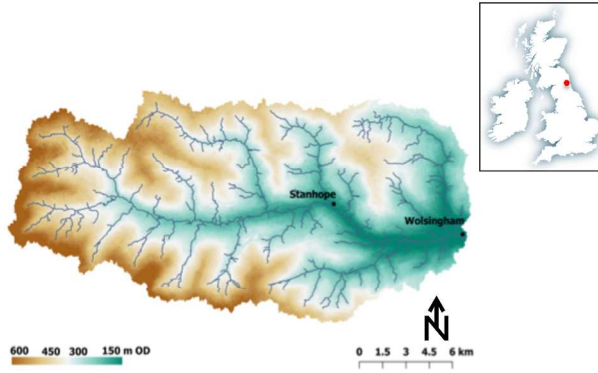
52
53
54 Table 1. Comparison of measured and simulated water elevations for the study
55 reach (m)
56
57
58
59
60

Table 1. Comparison of measured and simulated water elevations for the study reach (m).

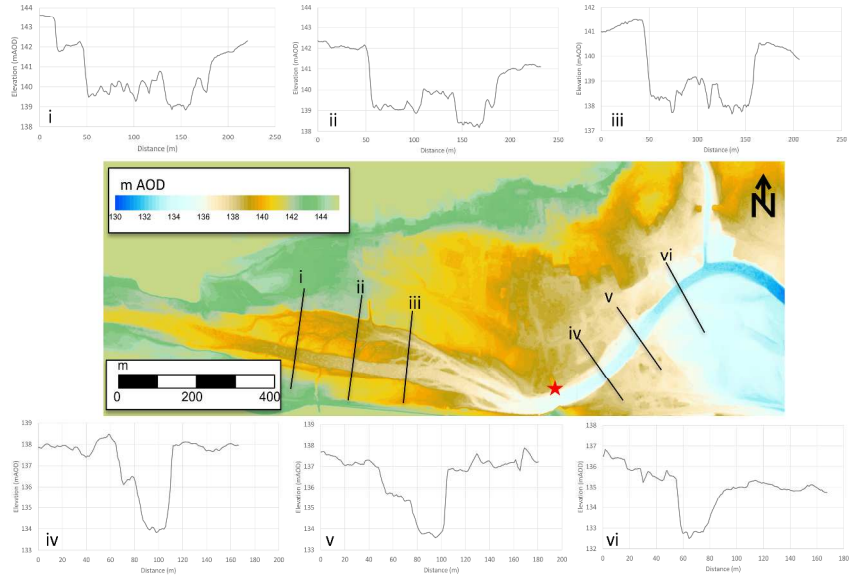
| | | Upstream | Mid | Downstream |
|--|----------|-----------------|------------|-------------------|
| Q = 5.2 m ³ s ⁻¹ 04/08/2012 | Measured | 140.04 | 138.12 | 133.86 |
| | Modelled | 140.029 | 138.107 | 133.889 |
| | Error | -0.011 | -0.013 | 0.029 |
| Q = 7.8 m ³ s ⁻¹ 05/08/2012 | Measured | 138.58 | 138.11 | 133.25 |
| | Modelled | 138.581 | 138.093 | 133.248 |
| | Error | 0.001 | -0.017 | -0.002 |

1
2
3
4
5
6
7
8
9
10
11
12
13
14
15
16
17
18
19
20
21
22
23
24
25
26
27
28
29
30
31
32
33
34
35
36
37
38
39
40
41
42
43
44
45
46
47
48
49
50
51
52
53
54
55
56
57
58
59
60

a)

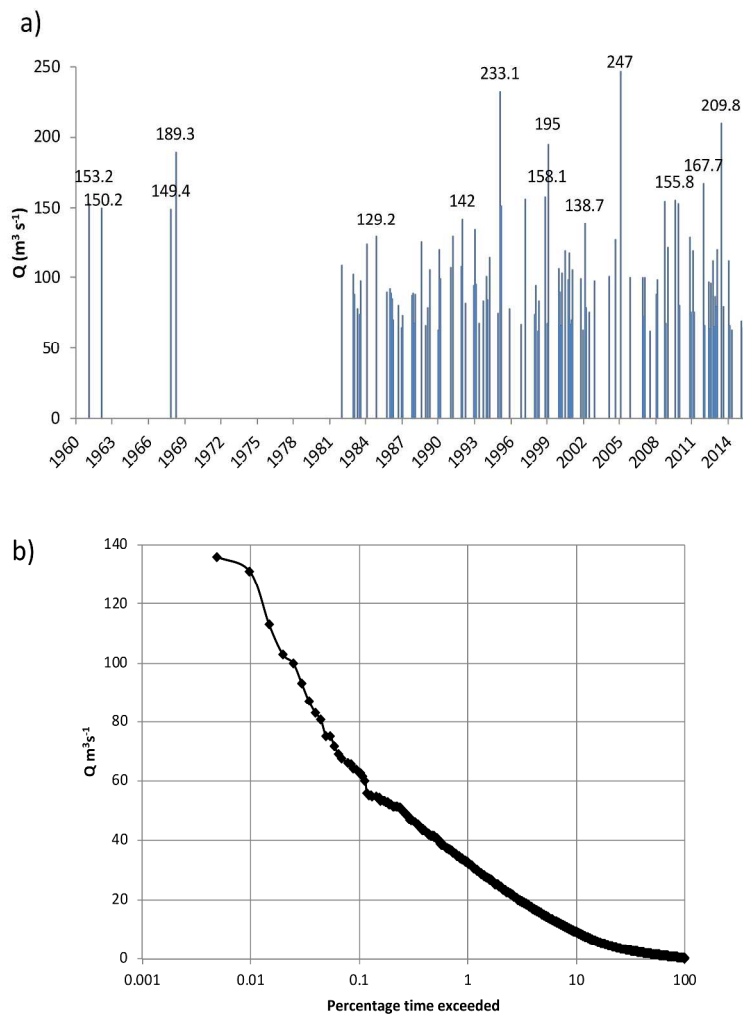


b)



F1

629x891mm (200 x 200 DPI)



F2

Figure 2.

629x891mm (200 x 200 DPI)

Unable to Convert Image

The dimensions of this image (in pixels) are too large to be converted. For this image to convert, the total number of pixels (height x width) must be less than 40,000,000 (40 megapixels).

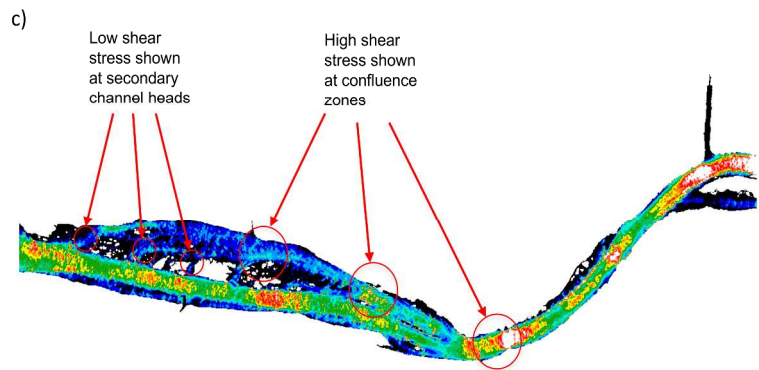
For Peer Review

Unable to Convert Image

The dimensions of this image (in pixels) are too large to be converted. For this image to convert, the total number of pixels (height x width) must be less than 40,000,000 (40 megapixels).

For Peer Review

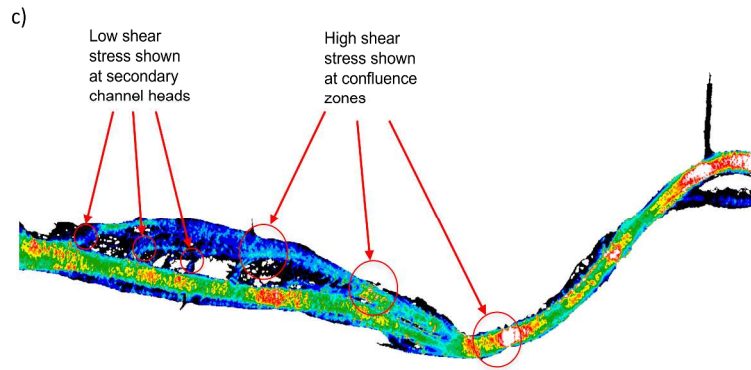
1
2
3
4
5
6
7
8
9
10
11
12
13
14
15
16
17
18
19
20
21
22
23
24
25
26
27
28
29
30
31
32
33
34
35
36
37
38
39
40
41
42
43
44
45
46
47
48
49
50
51
52
53
54
55
56
57
58
59
60



F6

826x1169mm (96 x 96 DPI)

1
2
3
4
5
6
7
8
9
10
11
12
13
14
15
16
17
18
19
20
21
22
23
24
25
26
27
28
29
30
31
32
33
34
35
36
37
38
39
40
41
42
43
44
45
46
47
48
49
50
51
52
53
54
55
56
57
58
59
60



F6

440x623mm (200 x 200 DPI)

1
2
3
4
5
6
7
8
9
10
11
12
13
14
15
16
17
18
19
20
21
22
23
24
25
26
27
28
29
30
31
32
33
34
35
36
37
38
39
40
41
42
43
44
45
46
47
48
49
50
51
52
53
54
55
56
57
58
59
60



F3

Figure 3.

629x891mm (200 x 200 DPI)

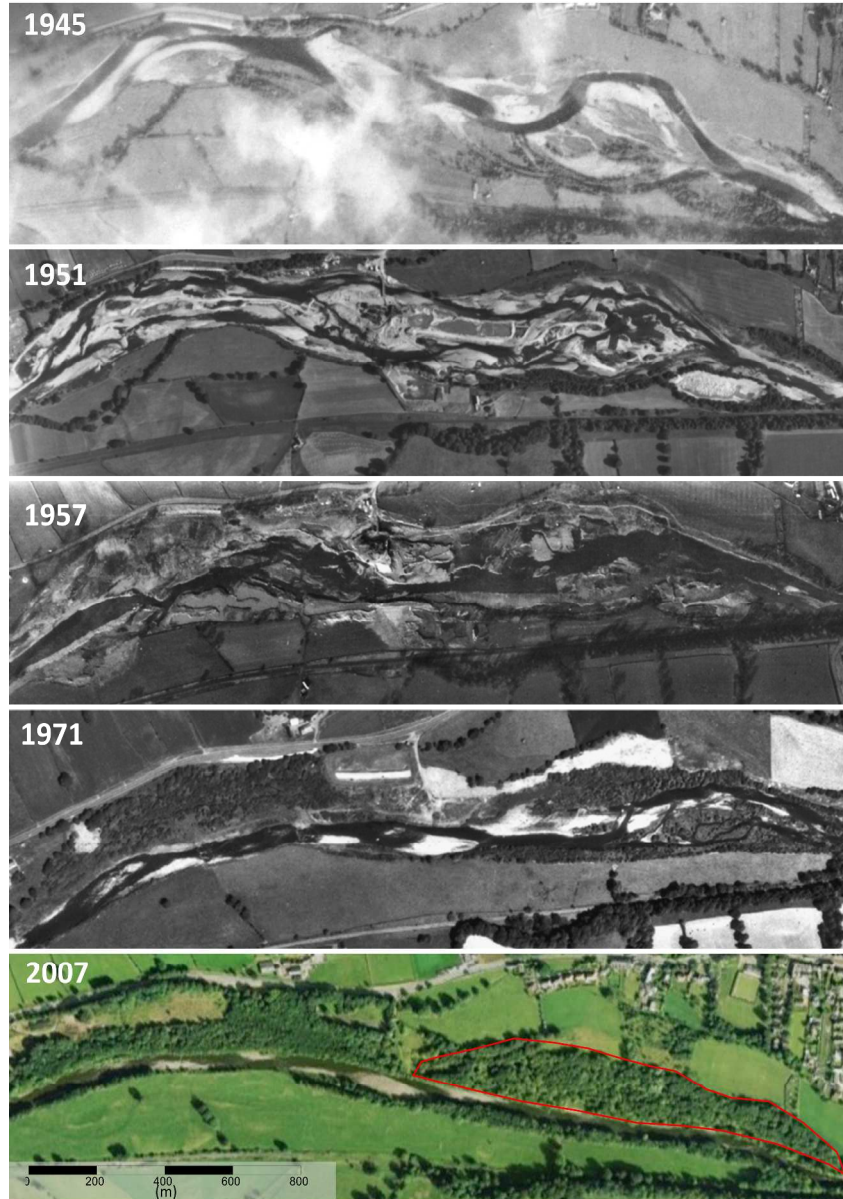


Figure 4.

629x891mm (200 x 200 DPI)

1
2
3
4
5
6
7
8
9
10
11
12
13
14
15
16
17
18
19
20
21
22
23
24
25
26
27
28
29
30
31
32
33
34
35
36
37
38
39
40
41
42
43
44
45
46
47
48
49
50
51
52
53
54
55
56
57
58
59
60



Figure 5A.

629x891mm (200 x 200 DPI)

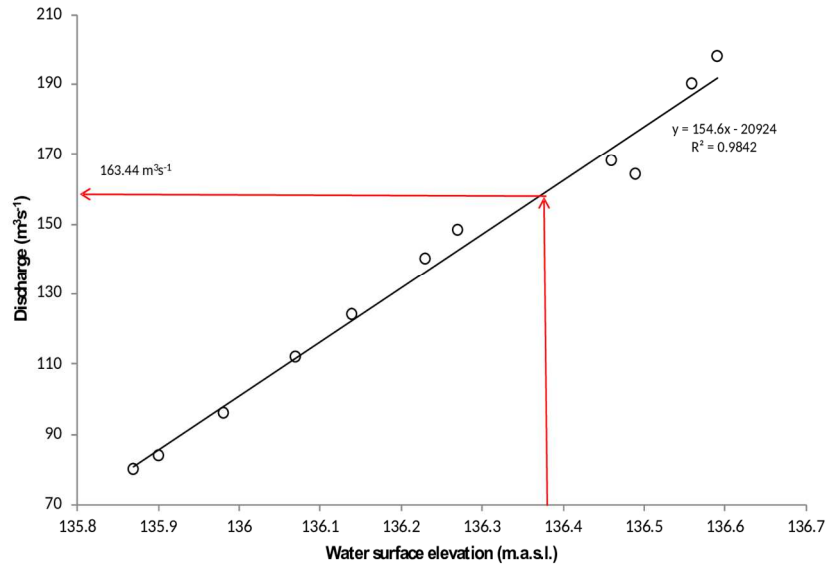


Figure 5B.

629x891mm (200 x 200 DPI)

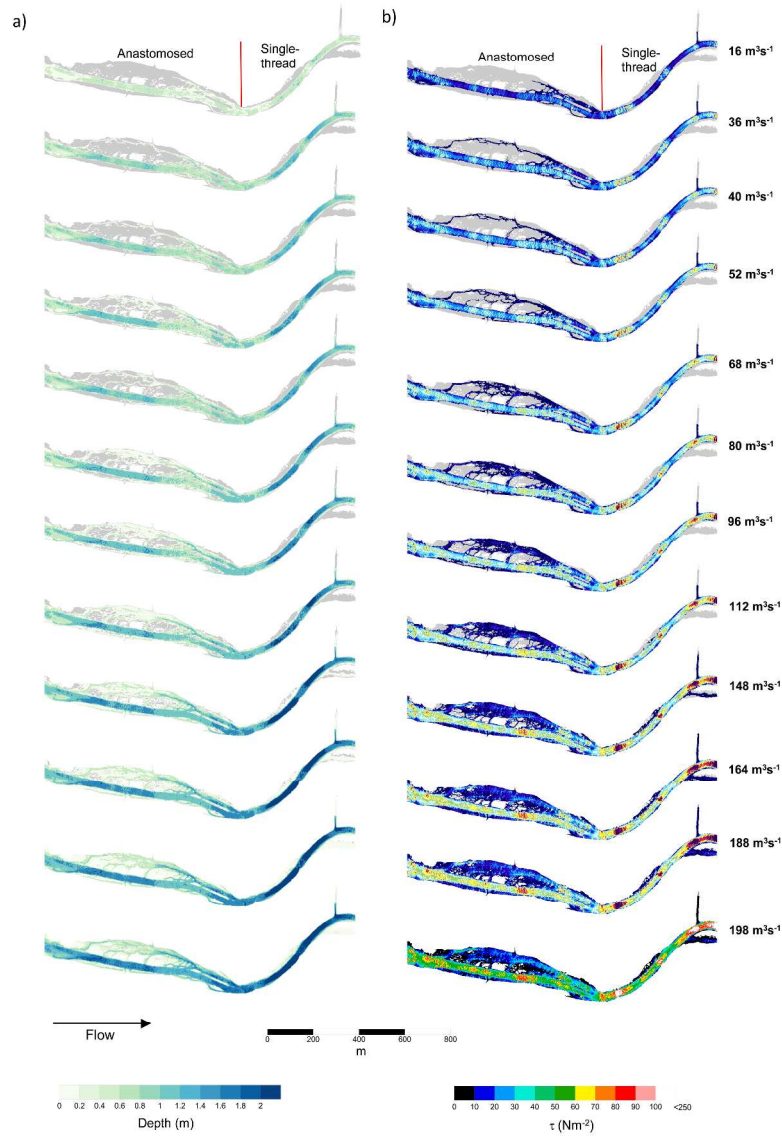
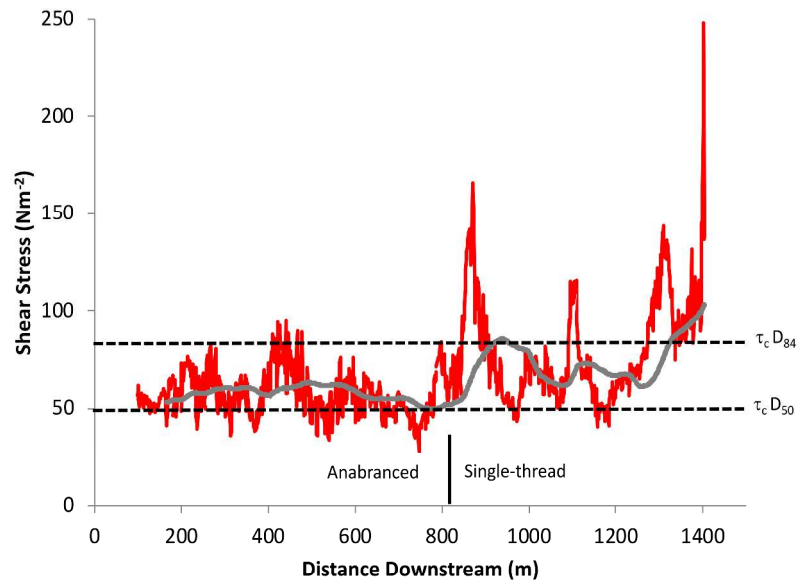


Figure 6AB.

629x891mm (200 x 200 DPI)

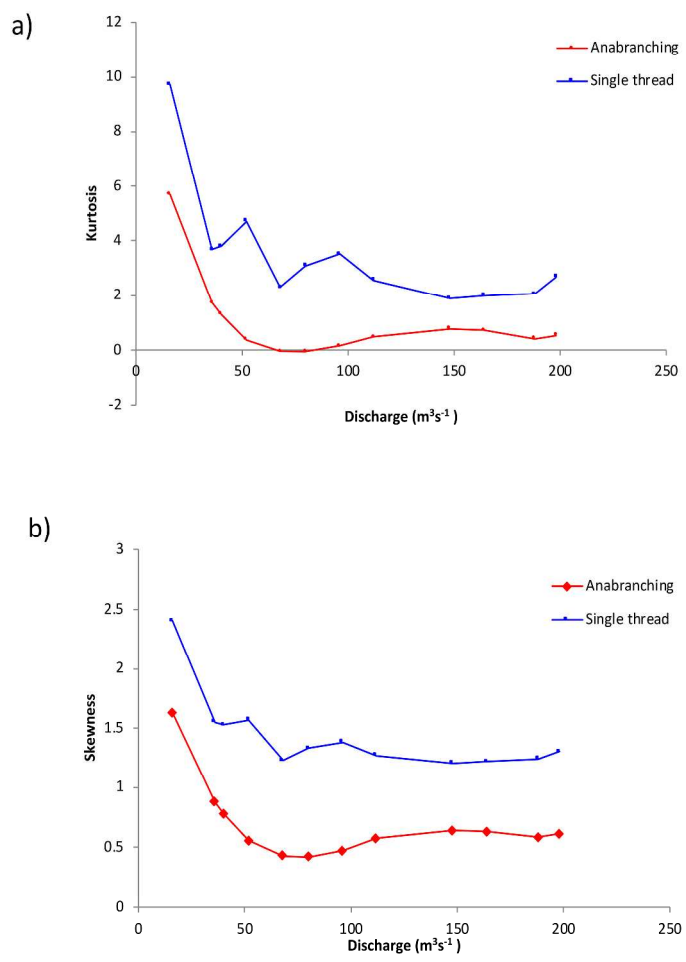


F7

Figure 7.

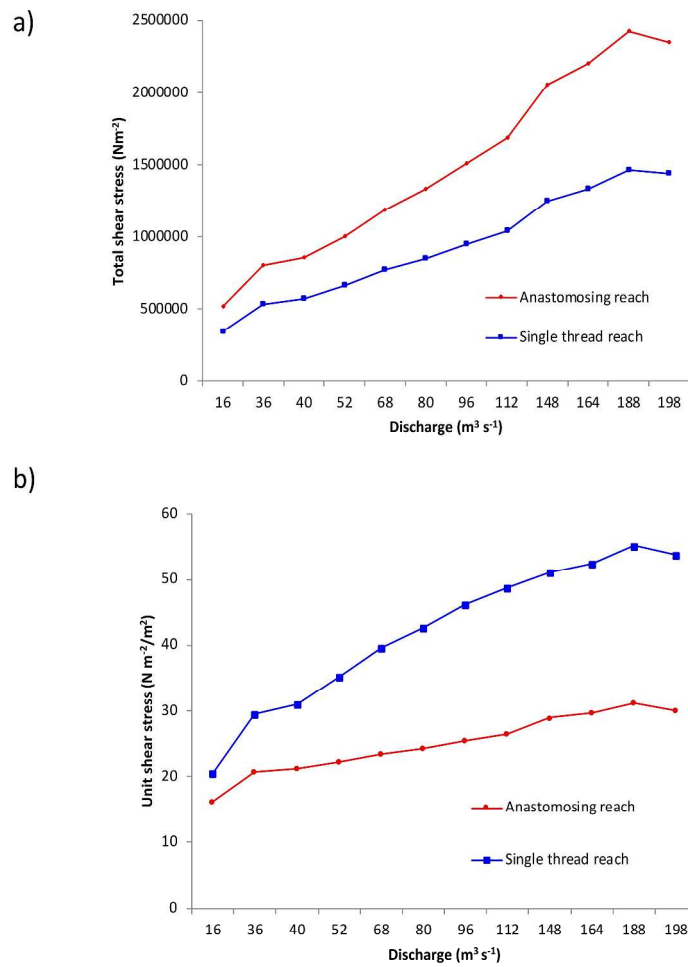
629x891mm (200 x 200 DPI)

1
2
3
4
5
6
7
8
9
10
11
12
13
14
15
16
17
18
19
20
21
22
23
24
25
26
27
28
29
30
31
32
33
34
35
36
37
38
39
40
41
42
43
44
45
46
47
48
49
50
51
52
53
54
55
56
57
58
59
60



F8

Figure 8.
629x891mm (200 x 200 DPI)



F9

Figure 9.

629x891mm (200 x 200 DPI)

1
2
3
4
5
6
7
8
9
10
11
12
13
14
15
16
17
18
19
20
21
22
23
24
25
26
27
28
29
30
31
32
33
34
35
36
37
38
39
40
41
42
43
44
45
46
47
48
49
50
51
52
53
54
55
56
57
58
59
60

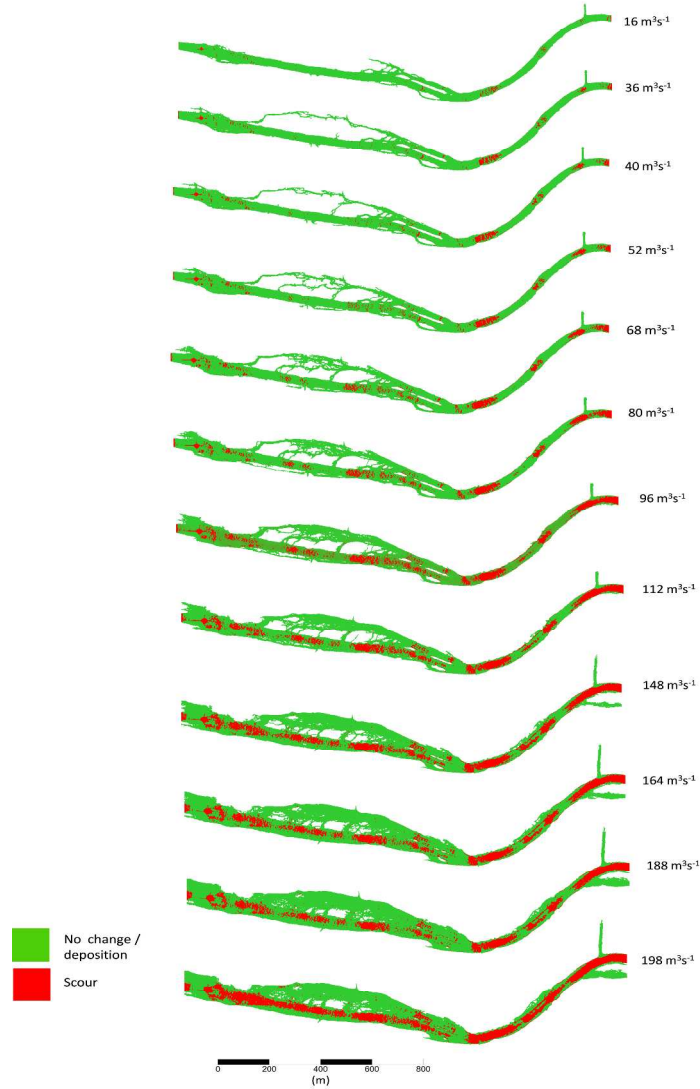


Figure 10.

629x891mm (200 x 200 DPI)